

End-to-End Text Line Detection and Ordering

Benjamin Kiessling^[0000-0001-9543-7827]

ALMAnaCH, Inria, France

Abstract. Practical text-recognition pipelines for historical documents typically decompose layout analysis into line detection followed by a separate reading-order step, with the latter most often handled by a hand-coded geometric heuristic that struggles with marginalia, multiple columns, tables, and source-specific editorial conventions. This article introduces Orli (Ordered Regression of Lines), an end-to-end model that casts both sub-tasks as a single image-to-sequence problem: from a page image, Orli autoregressively generates text-line baselines directly in reading order. Baselines are represented in a chord-frame parameterization that anchors a line’s position, orientation, and extent while encoding local geometry through perpendicular offsets; an iterative refinement head and a local visual refiner produce the final curve. Trained on a heterogeneous corpus of 196,691 pages spanning ten writing systems, Orli marginally exceeds the previously reported state of the art for cBAD line detection without dataset-specific training, reaches near-perfect coverage and ordering on multiple reading-order benchmarks zero-shot, and adapts to more specialized out-of-domain layouts with limited fine-tuning. The method’s source code and model weights are available under an open license at <https://github.com/mittagessen/orli>.

Keywords: layout analysis · reading order determination · historical document analysis

1 Introduction

Segmentation-free and full-page text recognizers have made rapid progress in recent years, showing that handwritten paragraphs or whole pages can be transcribed without an explicit line-segmentation stage [31, 6, 7], with recent vision-language models extending the same idea to structured full-page document recognition with implicitly learned reading order [4, 26]. Nevertheless, practical text-recognition pipelines for historical material are still commonly structured around two separate steps: layout analysis, usually in the form of line detection, followed by line-level recognition. This is not simply a question of new methods awaiting adoption. Historical collections often provide modest amounts of task-specific training data, cover long-tail languages, scripts, orthographies, hands, and document genres, and are used in scholarly settings where silent normalization or hallucinated text can be more damaging than overt recognition errors. Line-based pipelines are better suited to these constraints than specialized VLMs for automatic text recognition or OCR-capable general-purpose LLMs, and they

offer a degree of introspection and control that remains important in practice: detected lines can be inspected, corrected, selectively ignored, or passed to recognizers and downstream tools with collection-specific assumptions.

In current practice, however, layout analysis itself is usually split into two sub-tasks: line segmentation, which produces an unordered set of lines, and reading order determination, which arranges them into a reading sequence. The two sub-tasks are typically handled by separate components, and progress on them has been uneven. Line detection has matured into a relatively robust technology over the past decade, whereas reading order is still most often delegated to a heuristic post-processor that operates on the already-detected lines.

This separation is convenient, but it treats ordering as a simple geometric property of the page. In historical documents this assumption is often too narrow. Marginalia, additions, interlinear notes, multiple columns, tables, page numbers, commentary layers, and source-specific editorial conventions can all determine whether a line should be read, when it should be read, or whether it should be ignored for a particular transcription. As with line segmentation, different scholarly uses of the same page may therefore imply different reading orders. A marginal addition with an insertion mark, for example, may be integrated into the main text at the indicated point in one transcription norm and read as a separate apparatus block at the end of the page in another, even though the page itself is unchanged. Hand-coded sorting rules can express only a small subset of these decisions.

This motivates a formulation in which the layout-analysis output is an ordered sequence rather than a set of lines paired with a separate sorting rule. A model that emits one line at a time, autoregressively, makes both decisions in a single pass: each generated element specifies a line, and the order in which elements are emitted specifies the reading order. Ordering then becomes a supervised visual prediction problem trained jointly with detection rather than a collection-specific post-processing rule applied after the fact.

This article introduces Orli, Ordered Regression of Lines, an end-to-end layout-analysis model for historical documents. Orli treats page layout as an image-to-sequence problem: from a page image, it generates text-line baselines directly in reading order. The main contribution is therefore a joint formulation of text-line detection and reading-order determination in which both the geometry of the lines and their sequence are learned from the same visual input. The article presents the model, its baseline representation and geometric refinement strategy, and evaluates the resulting system on heterogeneous historical material and public layout-analysis benchmarks.

2 Related Work

2.1 Segmentation-Free Recognition and Line-Based Pipelines

Segmentation-free handwriting recognition methods challenge the classical assumption that a document must first be segmented into individual text lines.

Start-Follow-Read introduced a full-page recognizer that alternates between locating a reading position and recognizing text from it [31]; attentional networks have since shown strong results on paragraph- and page-level handwritten text recognition without an explicit line-segmentation stage [6, 7]. More recently, large vision-language models and OCR-specialized VLMs have extended this idea to structured full-page document recognition. Examples of these kinds of models are the Qwen3-VL general-purpose VLM with long-context multimodal document capabilities and OCR-oriented training [4], and LightOnOCR-2-1B for end-to-end multilingual document image-to-text conversion with naturally ordered output [26].

These systems demonstrate that recognition, ordering, and implicit layout modeling can be learned jointly, but they also shift a large part of the layout problem into the recognizer or VLM itself. For historical document analysis this is not always desirable: the relevant language, script, transcription norms, or document genre may be low-resource; the recognizer may require more data or computation than a project can provide; and the resulting text output is harder to audit than a line-based intermediate representation. Recent empirical work substantiates these concerns. State-of-the-art VLMs underperform dedicated systems on highly structured historical material in zero-shot settings and depend on fine-tuning to recover competitive accuracy [2], and even when their aggregate character- or word-error rates are favourable they exhibit selective linguistic regularization and orthographic normalization that may silently alter historically meaningful forms [29].

2.2 Text Line Segmentation

Line-based pipelines instead keep document geometry explicit, and text-line detection has long been a central task in historical document analysis [17]. What a “line” actually is varies across systems, and the choice of data model shapes both the methods that can be applied and the form in which lines are passed to downstream recognition. Three representations are commonly used: axis-aligned bounding boxes, which are simple but poorly suited to curved or rotated handwriting; bounding polygons, which fit the writing area more faithfully but are difficult to normalize to a consistent line-level scale; and baseline polylines, which isolate a one-dimensional curve along the writing direction and have become the most common representation for historical layout analysis, as they are compact, support normalization into a flat strip, and exist naturally in most common writing systems.

Early methods for recovering any of these representations relied on binarization, connected components, projection profiles, seam carving, or other image-processing operations whose assumptions had to be adapted to each document family. Contemporary work is dominated by neural approaches that fall into two broad families.

The first and by far the most common family is specific to baseline detection and treats it as an instance segmentation task solved via semantic segmentation: a network labels pixels as baselines, and a post-processing stage clusters

the resulting maps into baseline instances. Representative systems [12, 3, 13] differ primarily in the underlying segmentation architecture, ranging from convolutional encoder-decoders to recurrent variants and, more recently, attention-based segmentation networks, in the presence of auxiliary classes that aid in line separation or orientation detection, and in the sophistication of the baseline-instance extraction step. The standard public benchmark for this family is the cBAD competition with its accompanying dataset, which established baseline detection as a practical task for archival documents and introduced an evaluation protocol suited to baseline polylines [9, 11].

A second, more recent family adopts direct set prediction, regressing abstract line entities from the image without an intermediate pixel-level stage. Standard object-detection architectures have been applied to historical text-line detection on suitable collections [28], but their use is restricted to material whose lines exhibit limited curvature, comfortable inter-line spacing, and consistent orientation; properties that a general-purpose layout analysis system cannot assume. Adapting these detectors to better-suited line data models is also difficult, because they bake the bounding-box model deeply into their design, from anchor priors and non-maximum suppression down to the regression head. The DETR family [5] is more flexible: by replacing anchor priors and non-maximum suppression with direct box parameter regression, it makes alternative geometric heads easier to introduce. CurT illustrates this flexibility by replacing bounding-box regression with cubic Bézier-curve regression for baseline detection [14]. The main drawbacks remain long training schedules, large training-data requirements, and high computational cost. Recent variants such as DAB-DETR and RT-DETR [19, 33] mitigate these issues, but partly through reintroducing box-centered mechanisms such as dynamic anchors and query selection.

Despite their differences, both segmentation-based and set-prediction methods produce line instances before ordering is considered. Orli sits within the direct-regression family in that it predicts abstract baselines without an intermediate pixel-labelling stage, but it differs from set-based detectors by generating baselines autoregressively. The generated sequence is therefore both the detection result and the reading order.

2.3 Reading Order Determination

Reading order determination remains an under-addressed problem in the document-analysis literature, and in the absence of broadly applicable learnable methods it is most often delegated to geometric heuristics: elements are grouped into regions or columns and sorted according to a preferred direction. This is transparent and efficient, but it externalizes much of the real work into manually designed assumptions about the collection and fails on complex pages; a state of affairs that has changed little since Quirós and Vidal made the same observation in 2022 [24]. They proposed one of the few dedicated trainable approaches for handwritten documents, learning order relations over layout elements and releasing datasets for evaluating reading-order methods in this setting. Their

work is especially relevant here because it treats reading order as a document-analysis problem rather than as a purely textual problem, but it still operates over already-detected layout elements.

In visually rich modern documents, reading order has also been studied as a post-OCR or multimodal task. LayoutReader pre-trains on text and layout to recover the reading order of OCR tokens [30]; other work formulates OCR text reorganization as a sequence-learning task or predicts pairwise ordering relations from visual, textual, and layout information [16, 21]. These methods show that learned ordering can outperform simple geometric rules, but their assumptions transfer poorly to the historical line-detection setting considered here. They typically operate over already-recognized text blocks with bounding boxes and therefore require full OCR output before ordering can take place. More fundamentally, the textual half of these models is almost always a pre-trained large language model, which restricts their applicability to high-resource modern languages and scripts; for the long tail of historical languages, hands, orthographies, and non-Latin scripts that motivate this work, comparable pre-trained models are rarely available, and even where they exist their compute and training-data requirements are poorly matched to the modest annotation budgets typical of historical research.

3 Method

3.1 Task Formulation

Given a document page image I , our method emits a variable-length sequence y_1, y_2, \dots, y_T in which each token $y_t = (c_t, \mathbf{x}_t)$ consists of a class decision c_t and a curve vector \mathbf{x}_t . The vocabulary contains four token classes: a beginning-of-sequence token (BOS), an end-of-sequence token (EOS), a line token (LINE), and a padding class used only inside batched tensors. For a LINE token the curve vector encodes a single text-line baseline; in all other cases it is unused. The sequence is generated autoregressively with the order in which LINE tokens are produced representing the reading order.

3.2 Architecture Overview

Orli has three components: a visual encoder backbone, a hybrid encoder feature fusion block, and an autoregressive decoder with an attached curve regression head. Figure 1 shows the overall data flow.

Backbone A ConvNeXtV2 (tiny variant) backbone [32] initialised with the `timm convnextv2_tiny.fcmae_ft_in22k_in1k` weights is applied to the input image. The three feature maps with output strides 8, 16, and 32 are forwarded to the hybrid encoder without further pooling.

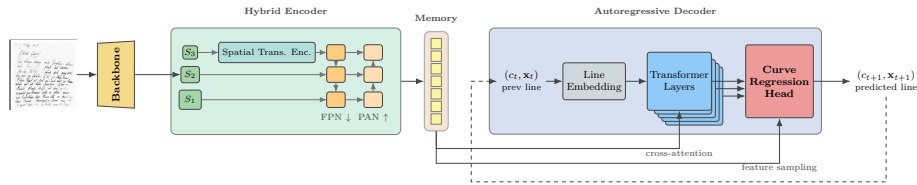


Fig. 1. Overall architecture of Orli. The curve regression head’s internals are detailed in Figure 3.

Hybrid encoder Multi-scale features are projected to a shared channel dimension of 256 and fused into a single sequence of memory tokens. The design follows the hybrid encoder of RT-DETR [33]: the deepest selected scale (stride 32) is refined by a single spatial transformer encoder layer with 2D sine-cosine positional embeddings, then a top-down feature-pyramid pathway followed by a bottom-up path-aggregation pathway [20] propagate context across scales. Per-level outputs are flattened, projected to the decoder embedding dimension, augmented with 2D sine-cosine positional embeddings and a learned level embedding, and concatenated into the final memory token sequence.

Decoder A LLaMA-style transformer [27] of 12 layers with embedding dimension 576 and intermediate dimension 1536. Each layer combines causal self-attention with rotary position embeddings [25] and grouped-query attention [1] (9 query heads, 3 key/value heads), followed by an unmasked cross-attention sub-layer that attends from decoder positions to the encoder memory. Token inputs are formed by a dedicated embedding module that projects the one-hot class part and the curve part separately and sums the two projections. In addition to the final hidden state, the decoder exposes intermediate hidden states from three earlier layers (L_2, L_5, L_8); these four states feed the curve regression head.

3.3 Curve Regression Head

The curve regression head turns the four tapped decoder hidden states into a baseline curve in two stages: an anchor-initialised iterative refinement that operates in the curve’s parameter space, followed by a local visual refiner that conditions a final correction on encoder features sampled along the predicted line. Figure 3 shows the head as a whole.

Curve representation. A baseline is described by its endpoint chord together with a local frame attached to it. Let \mathbf{c} be the chord midpoint, L the chord length, $\mathbf{u} = (\cos \theta, \sin \theta)$ the chord direction, and \mathbf{n} its 90° rotation. The chord is sampled at $K = 16$ equally spaced positions $\mathbf{b}_i = \mathbf{c} + (s_i - \frac{1}{2})L\mathbf{u}$ with $s_i = i/(K - 1)$, and the baseline geometry is encoded as the signed perpendicular distance from each \mathbf{b}_i to the corresponding point on the curve along the normal direction \mathbf{n} . The

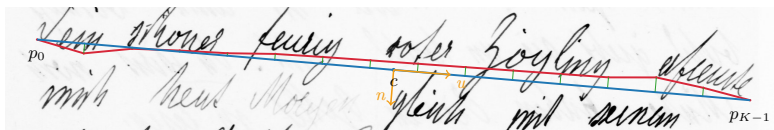


Fig. 2. Chord-based local-frame representation on a historical baseline from cBAD (cPAS-0423).

trainable curve vector concatenates the chord parameters with these K normal offsets,

$$\mathbf{x} = (c_x, c_y, L/\sqrt{2}, \frac{1+\sin\theta}{2}, \frac{1+\cos\theta}{2}, d_0, \dots, d_{K-1}),$$

where each $d_i \in [0, 1]$ is the affine remapping of that signed distance. Image coordinates are normalized to $[0, 1]^2$, the divisor $\sqrt{2}$ is the diagonal of the unit square, so $L/\sqrt{2} \in [0, 1]$ for any chord; all entries are then bounded in $[0, 1]$, which makes them compatible with the sigmoid-space refinement scheme used below. Decoding to a polyline evaluates

$$\mathbf{p}_i = \mathbf{c} + (s_i - \frac{1}{2}) L \mathbf{u} + d_i \mathbf{n}, \quad s_i = i/(K - 1).$$

This parameterization builds part of the expected line structure into the regression target. Direct point regression places no smoothness prior on the output: each sample is predicted independently and small per-point errors can accumulate into a visibly jittery polyline on high-curvature lines. Bézier control points impose a stronger curve model, but are not in general co-located with the decoded curve, so the regression target lies away from the geometry it controls. The chord frame provides an intermediate representation: the chord anchors the line’s position, orientation, and extent while staying close to the line itself, and the normal offsets describe local deviations from that coarse support. This keeps the target flexible enough for historical baselines while making consistency along the line easier to learn. Figure 2 illustrates the representation on a historical baseline.

Iterative refinement The head refines the curve over four iterations. Each iteration t takes the current curve state $\mathbf{x}^{(t)}$ and a decoder hidden state $\mathbf{h}^{(t)}$ tapped from a fixed layer (in order: L_2, L_5, L_8, L_{12}) and predicts a logit-space offset $\delta^{(t)}$ from a concatenation of $\mathbf{h}^{(t)}$ and a linear projection of $\text{logit}(\mathbf{x}^{(t)})$. The next curve state is

$$\mathbf{x}^{(t+1)} = \sigma(\text{logit}(\mathbf{x}^{(t)}) + \delta^{(t)}),$$

so that every update stays in $[0, 1]$ and the curve is moved towards its target by additive offsets in logit space. Each offset MLP carries separate parameters that are zero-initialized to ensure the head starts as identity.

The first iteration is preceded by an anchor-based initialization: a fixed table of $N = 8$ anchor curves, mined from the training distribution by clustering resampled training baselines in chord-frame space; from $\mathbf{h}^{(1)}$ an anchor selector

predicts a categorical distribution over the anchors, and the selected anchor’s curve vector becomes the initial state $\mathbf{x}^{(0)}$ that the first offset MLP refines. All four iteration outputs contribute equally to the curve regression loss.

Local visual refiner The first-stage iterative refinement receives visual evidence through decoder cross-attention over the full encoder memory. This global context is useful for locating and shaping a line, but it gives the regression head no explicit local view of the pixels immediately around the predicted baseline.

In preliminary experiments, residual errors often appeared as local alignment drift: the predicted curve followed the text line but shifted within the writing body, sometimes toward a centerline rather than the annotated baseline. The local visual refiner targets this final alignment step. After the last refinement step the curve is decoded to its K polyline points; at each point,

encoder features are bilinearly sampled from every memory level, augmented with per-point positional embeddings, and concatenated across levels into a single set of $K \cdot M$ local tokens per line, where M is the number of encoder levels. The decoder hidden state $\mathbf{h}^{(4)}$ acts as a single query attending over this local token set via 8-head multi-head attention. The attention output is concatenated with $\mathbf{h}^{(4)}$ and the logit-space projection of $\mathbf{x}^{(4)}$, passed through a small MLP whose final layer is again zero-initialized, and added in logit space as a correction:

$$\mathbf{x}^{\text{refined}} = \sigma(\text{logit}(\mathbf{x}^{(4)}) + \delta^{\text{refiner}}).$$

The refiner is therefore not a second detector. It leaves the generated line identity and coarse geometry unchanged and predicts only a final correction in the same parameter space, using visual features sampled where the line is currently estimated to be. A single iteration is used because the module is intended

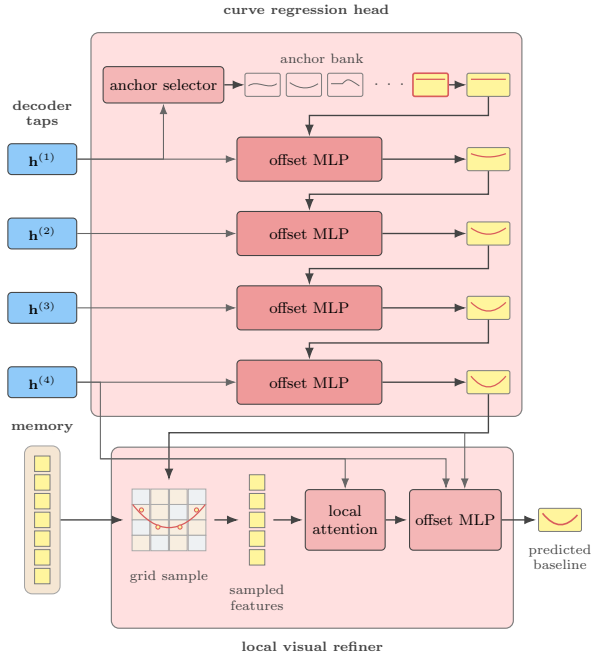


Fig. 3. Curve regression head and local visual refiner.

to correct residual alignment errors, while repeated local attention would add cost at every generated line.

3.4 Training Objective

The total loss combines token-classification, anchor-classification, and curve-regression terms,

$$\mathcal{L} = \mathcal{L}_{\text{cls}} + \mathcal{L}_{\text{anc}} + \mathcal{L}_{\text{poly}} + \mathcal{L}_{\text{param}},$$

all of which are summed and minimized jointly; no loss balancing is applied beyond the per-target normalizers described below, as preliminary experiments with hand-tuned weights did not yield improvements.

The token-classification loss \mathcal{L}_{cls} is a focal loss [18] with focusing parameter $\gamma = 2$ over the four mutually exclusive token classes, applied at every iterative refinement step and averaged over steps.

The anchor-classification loss \mathcal{L}_{anc} is a likewise focal loss with $\gamma = 2$ and $\alpha = 0.25$ over the anchor table. For each LINE token, the target anchor is the table entry whose decoded polyline is closest in ℓ_1 distance to the ground-truth polyline; the remaining anchors are treated as negatives.

The curve-regression loss is the sum of two ℓ_1 terms applied to every iteration’s output: a polyline term $\mathcal{L}_{\text{poly}}$ comparing the decoded polyline to the ground-truth polyline, and a parameter term $\mathcal{L}_{\text{param}}$ comparing the raw curve vector \mathbf{x} to the ground-truth parameter vector. The polyline term supervises the geometry that is evaluated and passed downstream. The parameter term regularizes the chord-frame decomposition used by the iterative head, so that the model does not have to infer stable combinations of chord position, orientation, length, and offsets only from decoded sample points. Together, the two terms supervise both the represented curve and the internal variables through which the curve is refined. The contributions of all refinement iterations are averaged, and the final refined curve produced by the local visual refiner is included in the same aggregation.

3.5 Training and Inference

For the ablation study and the low-resolution base model, input images are normalized and resized to 1280×960 pixels in a non-aspect-ratio-preserving manner. The high-resolution base model used in the benchmark experiments is trained at 1920×1440 pixels. In all cases, target baselines are resampled to $K = 16$ points.

Unless otherwise stated, models are trained with bf16-mixed precision and AdamW (10^{-4} weight decay) on three A40 GPUs. The initial learning rate is 5×10^{-4} , decayed by a cosine schedule to 5×10^{-6} after a 1000-step linear warmup. The per-device batch size is 12, with two gradient accumulation steps for an effective batch size of 24. Training images are augmented with pixel dropout, color jitter, random conversion to grayscale, blur, and coarse dropout.

At inference, generation is greedy and runs until EOS is emitted.

4 Experiments

4.1 Data and Training Protocols

The base model is trained on a heterogeneous composite corpus with two components. The first consists of randomly sampled pages of rendered arXiv articles, which supply structured multi-column scientific layouts together with reliable baseline annotations recovered from the rendering pipeline. The second consists of real-world handwriting and print corpora drawn from a variety of sources, which provide the layout heterogeneity and annotation diversity characteristic of historical material. The full list of constituent datasets is provided as part of the open software distribution of the method¹.

The corpus comprises 196,691 training pages, 1,919 validation pages, and 1,914 test pages. Validation and test pages are sampled randomly within each language, with each held-out split capped at the smaller of 100 pages or 5% of that language’s training pages. Its natural portion is deliberately heterogeneous, ranging from twentieth-century correspondence and administrative records to printed books, stenographic shorthand, and highly fragmentary Genizah documents. Roughly a quarter of the training pages (49,095; 25.0%) are arXiv-derived synthetic renderings of English-language academic text; the remaining 147,596 natural pages span ten writing systems, with the breakdown by script and language given in Table 1.

Table 1. Composition of the natural-document portion of the training corpus by script and language. Percentages refer to the full 196,691-page training set; the remaining 25.0% (49,095 pages) are arXiv-derived synthetic renderings.

Script	Languages (pages each)	Pages (%)
Latin	Dutch (19,075), German (16,274), Swedish (11,326), Norwegian (11,087), Middle French (6,885), Portuguese (6,646), English (6,217); long tail down to fewer than 50 pages each for Picard, Occitan, Corsican	100,935 (51.3%)
Hebrew	Hebrew (28,170), Yiddish (1,702)	29,872 (15.2%)
Cyrillic	Russian (4,466), Church Slavonic (3,047), Ukrainian (697)	8,210 (4.2%)
Arabic	Arabic (4,301), Urdu (1,191), Persian (859), Ottoman Turkish (315)	6,666 (3.4%)
Other	Syriac (804), German stenographic shorthand (630), Ancient Greek (252), Georgian (183), Malayalam (44)	1,913 (1.0%)

The held-out split of the composite corpus is used to measure broad transfer across the heterogeneous training distribution. Because the constituent datasets were created with different annotation goals, missing marginalia, secondary lines, or collection-specific line definitions can affect both detection and ordering scores.

¹ redacted

High scores on this test set are therefore best read as evidence of generalization in a highly diverse setting.

For line-detection benchmarking, we use the cBAD 2019 test set [10], which contains primarily European historical handwritten documents annotated with baseline polylines. We report the base model without dataset-specific adaptation and a model fine-tuned on the corresponding cBAD training split. The comparison systems are the cBAD 2019 participants and the more recent ParseNet [15].

For reading-order benchmarking, we use three handwritten document datasets: OHG [23], FCR [22], and ABP [8], following the splits and line-at-page-level comparison protocol used by Quirós and Vidal [24]. OHG contains notarial records with mixed paragraph, marginal, and page-number regions; FCR contains Finnish court records, including both single- and double-page images with marginalia and tables; ABP is a table-heavy parish record dataset whose reading order is defined over dense cell and line structures. We report zero-shot Orli results on all three datasets and reserve fine-tuning for ABP, where the layout is furthest from the training mixture and the zero-shot model is weakest. Since Orli generates line geometry and order jointly, reading-order scores are computed on matched line instances and reported together with matched-line coverage.

4.2 Evaluation Metrics

Line detection is evaluated with the cBAD baseline-detection metric [11]. The metric first normalizes predicted and ground-truth baselines as polygonal chains and estimates a tolerance band for each ground-truth baseline from the local interline distance. Recall is the average coverage of ground-truth baselines by the predicted set under these tolerances. Precision is computed analogously after a greedy one-to-one alignment between predicted and ground-truth baselines, which penalizes segmentation errors such as splits and merges. The reported F1-score is the harmonic mean of precision and recall.

Reading order is evaluated with normalized Spearman footrule and Kendall’s τ . Let t_i and m_i be the ground-truth and predicted ranks of the i -th matched line among n matched lines. The normalized Spearman footrule is

$$F(t, m) = \frac{\sum_{i=1}^n |t_i - m_i|}{\lfloor n^2/2 \rfloor}.$$

Kendall’s τ is computed from the number of discordant line pairs $D(t, m)$,

$$\tau(t, m) = 1 - \frac{4D(t, m)}{n(n-1)}.$$

Both metrics are computed on matched line instances. We therefore report matched-line coverage alongside reading-order scores, defined as the fraction of ground-truth lines that could be paired with a predicted line before the ordering metric was computed.

Table 2. Architectural ablations on the held-out composite test set.

# Ablation	Precision	Recall	F1	Cov.	Footrule (\downarrow)	Kendall τ
1 Direct point prediction	0.9478	0.9470	0.9474	0.9584	0.0289	0.9662
2 Bézier curve prediction	0.9598	0.9587	0.9592	0.9665	0.0316	0.9638
3 Chord prediction	0.9192	0.9249	0.9220	0.9515	0.0315	0.9638
4 + Refiner	0.9660	0.9652	0.9656	0.9720	0.0323	0.9632
5 + 24 epochs	0.9672	0.9666	0.9669	0.9723	0.0288	0.9670
6 + high-res	0.9554	0.9564	0.9559	0.9667	0.0304	0.9649

5 Results

5.1 Ablation Study

Full training runs take approximately 32 hours on the hardware described in Section 3.5. The ablation study is therefore cumulative rather than factorial: starting from direct point regression, we replace the geometric representation, add the local visual refiner, extend the training schedule, and finally test a higher-resolution fine-tuning stage. Table 2 reports the resulting metrics on the held-out composite test set.

The chord parameterization on its own (row 3) falls below both direct point regression (row 1) and Bézier regression (row 2) on aggregate F1. These aggregates average over a line distribution dominated by mildly curved baselines on which all three parameterizations behave well; the failure modes of point and Bézier regression discussed in Section 3.3 affect a smaller, harder tail not visible in the aggregate score. Row 4 shows that once the local visual refiner supplies the offsets with sampled visual evidence, the chord representation’s structural advantages also translate into the best aggregate result.

Row 5 gives the best composite-corpus score, but the high-resolution model (row 6) is retained as the benchmark base because it transfers substantially better to the benchmark pages, where double-page scans in FCR, dense table layouts in ABP, and small secondary elements such as marginalia and page numbers make global downsampling more lossy.

5.2 Line-Detection Benchmarks

Table 3 compares Orli against baseline-detection systems on cBAD 2019. Scores are reported for the base model without adaptation and after fine-tuning on the cBAD training split. Since Orli emits lines in reading order, we additionally report matched-line coverage and reading-order metrics for the Orli variants.

The low-resolution base model transfers poorly to cBAD, reaching an F1-score of 0.7533 and matched-line coverage of 0.7781. Increasing the input resolution has a much larger effect than it did on the composite test set: the high-resolution base model reaches 0.9340 F1 with coverage rising to 0.9406. This

Table 3. Baseline-detection and reading-order comparison on cBAD 2019.

Method	Precision	Recall	F1	Cov.	Footrule (\downarrow)	Kendall τ
low-res base	0.7512	0.7554	0.7533	0.7781	0.0763	0.9101
high-res base	0.9378	0.9302	0.9340	0.9406	0.0768	0.9113
high-res fine-tuned	0.9395	0.9306	0.9351	0.9421	0.0720	0.9165
Planet [10]	0.937	0.926	0.931	–	–	–
DocExtractor [10]	0.920	0.931	0.925	–	–	–
DMRZ [10]	0.925	0.905	0.915	–	–	–
UPVLC [10]	0.911	0.902	0.907	–	–	–
ParseNet [15]	0.906	0.897	0.902	–	–	–

slightly exceeds the best previously reported single-system result on the benchmark, without any cBAD-specific training and with the model additionally producing an ordered sequence of baselines. The fine-tuned model achieves further although modest improvements. The footrule and Kendall τ values are computed only on matched lines, so they are not directly comparable across the low- and high-resolution models when coverage differs substantially.

5.3 Reading-Order Benchmarks

Table 4 reports results on the OHG, FCR, and ABP reading-order benchmarks. OHG and FCR contain historical records with line-level ordering phenomena such as marginalia, page numbers, additions, double-page scans, and nontrivial departures from simple top-to-bottom ordering. ABP is dominated by dense table structures and has substantially more lines per page. Orli is evaluated in its native detection-conditioned setting: it first generates baselines and then computes ordering metrics only on the matched subset of predicted and ground-truth lines. We therefore report matched-line coverage as explained above alongside the ordering scores.

The TBLR rows provide a simple top-to-bottom/left-to-right heuristic reference. The FDTD rows are the line-at-page-level results reported by Quirós and Vidal [24]: their MLP predicts pairwise order relations, and the First Decide Then Decode (FDTD) decoder converts the resulting relation matrix into a sequence. Both use existing line instances, so their ordering scores should be read together with Orli’s coverage rather than as direct end-to-end comparisons. For the high-resolution base model on OHG and FCR, coverage exceeds 0.99 and the matched subset is therefore essentially the full ground-truth set, so the bias from detection-conditioned ordering is negligible. For the low-resolution rows and for ABP, coverage is lower and the footrule and Kendall τ values should be read against the coverage column rather than in isolation.

For OHG and FCR, the high-resolution base model already reaches near-perfect coverage and strong ordering scores, so we do not report dataset-specific fine-tuning. ABP is a stronger domain shift: its table-cell reading order and large number of small line instances differ substantially from the base training mixture.

Table 4. Reading-order comparisons. TBLR and FDTD values are line-at-page-level results from [24].

Dataset Method		Line detection			Reading order		
		Prec.	Rec.	F1	Cov.	Footrule (\downarrow)	Kendall τ
OHG	low-res base	0.7218	0.7883	0.7536	0.8210	0.0210	0.9771
OHG	high-res base	0.9940	0.9937	0.9938	0.9993	0.0033	0.9967
OHG	TBLR [24]	–	–	–	–	0.0291	0.9667
OHG	FDTD [24]	–	–	–	–	0.0069	0.9913
FCR	low-res base	0.7994	0.8053	0.8023	0.8353	0.0210	0.9745
FCR	high-res base	0.9894	0.9874	0.9884	0.9905	0.0028	0.9971
FCR	TBLR [24]	–	–	–	–	0.3184	0.3978
FCR	FDTD [24]	–	–	–	–	0.0094	0.9840
ABP	low-res base	0.6067	0.6918	0.6464	0.7048	0.5238	0.3113
ABP	high-res base	0.8505	0.7919	0.8201	0.8071	0.5372	0.2878
ABP	high-res fine-tuned	0.8498	0.7806	0.8137	0.7931	0.0898	0.8972
ABP	TBLR [24]	–	–	–	–	0.1093	0.7790
ABP	FDTD [24]	–	–	–	–	0.0783	0.8359

We therefore report both the zero-shot high-resolution base model and an ABP fine-tuned model. Quirós and Vidal report Spearman footrule as percentages and Kendall distance as average absolute swaps; we divide footrule by 100 and convert Kendall distance to approximate Kendall τ using the average number of lines per page for each dataset.

6 Discussion

The benchmark experiments support the central premise of Orli: reading order can be learned as part of baseline generation rather than recovered by a separate post-processing stage. The strongest generalized model exceeds the previously reported state of the art for cBAD line detection without any cBAD-specific training, and at the same time produces an ordered sequence of line baselines. On OHG and FCR it reaches near-perfect matched-line coverage and very low reading-order error without benchmark-specific fine-tuning, showing that the same generalized model transfers well to these document families.

ABP, in contrast, is not solved zero-shot. Fine-tuning on its training split leaves detection F1 essentially unchanged but lifts the reading-order metrics by a large margin; detection on ABP is geometry-bound by the small, densely packed cell entries at the resolution used, whereas its reading order follows a dataset-specific traversal convention that the base model has no way to infer from the page alone. The base model can therefore be adapted to new document families and editorial ordering policies with limited additional data, without replacing the joint detection-and-ordering formulation.

7 Conclusion

Orli formulates historical page layout analysis as ordered baseline regression: a page image is mapped directly to a sequence of text-line baselines whose order defines the reading order. This preserves the inspectable line-based representation used by conventional OCR pipelines while making ordering a native part of the trainable prediction problem rather than a separate post-processing step.

The experiments show that this formulation is effective in both generalized and adapted settings. Without benchmark-specific fine-tuning, the generalized high-resolution model matches or marginally exceeds the previously reported state of the art for cBAD line detection and reaches near-perfect coverage and ordering performance on OHG and FCR. On ABP, a small and specialized out-of-domain benchmark, fine-tuning substantially improves the reading-order results, indicating that the base model can be adapted to new document families with limited additional data.

Taken together, these results position Orli as a bridge between conventional line-based text-recognition pipelines and modern transformer-based document models. It retains the flexibility and inspectability of explicit line detections, while giving both line geometry and reading order the modelling capacity of an integrated sequence prediction architecture.

Acknowledgements

This work was funded by the European Union under the ATRIUM project (Grant Agreement No. 101132163) and the ERC Synergy Grant MIDRASH (Grant Agreement No. 101071829). Views and opinions expressed are however those of the author only and do not necessarily reflect those of the European Union.

References

1. Ainslie, J., Lee-Thorp, J., De Jong, M., Zemlyanskiy, Y., Lebrón, F., Sanghai, S.: GQA: Training generalized multi-query transformer models from multi-head checkpoints. In: Proceedings of the 2023 Conference on Empirical Methods in Natural Language Processing. pp. 4895–4901 (2023)
2. Angleraud, N., Karamolegkou, A., Sagot, B., Clérice, T.: Structure-aware text recognition for ancient Greek critical editions. arXiv preprint arXiv:2603.02803 (2026). <https://doi.org/10.48550/arXiv.2603.02803>
3. Ares Oliveira, S., Seguin, B., Kaplan, F.: dhSegment: A generic deep-learning approach for document segmentation. In: 2018 16th International Conference on Frontiers in Handwriting Recognition. pp. 7–12. IEEE (2018). <https://doi.org/10.1109/ICFHR-2018.2018.00011>
4. Bai, S., Cai, Y., Chen, R., Chen, K., Chen, X., Cheng, Z., Deng, L., Ding, W., Gao, C., Ge, C., Ge, W., Guo, Z., Huang, Q., Huang, J., Huang, F., Hui, B., Jiang, S., Li, Z., Li, M., Li, M., Li, K., Lin, Z., et al.: Qwen3-VL technical report. arXiv preprint arXiv:2511.21631 (2025). <https://doi.org/10.48550/arXiv.2511.21631>

5. Carion, N., Massa, F., Synnaeve, G., Usunier, N., Kirillov, A., Zagoruyko, S.: End-to-end object detection with transformers. In: *Computer Vision – ECCV 2020*. pp. 213–229. Springer (2020). https://doi.org/10.1007/978-3-030-58452-8_13
6. Coquenot, D., Chatelain, C., Paquet, T.: End-to-end handwritten paragraph text recognition using a vertical attention network. *IEEE Transactions on Pattern Analysis and Machine Intelligence* **45**(1), 508–524 (2020). <https://doi.org/10.1109/TPAMI.2022.3144899>
7. Coquenot, D., Chatelain, C., Paquet, T.: DAN: A segmentation-free document attention network for handwritten document recognition. *IEEE Transactions on Pattern Analysis and Machine Intelligence* **45**(7), 8227–8243 (2022). <https://doi.org/10.1109/TPAMI.2023.3235826>
8. Déjean, H., Lang, E., Kleber, F.: READ ABP Table Datasets (2018). <https://doi.org/10.5281/zenodo.1243098>, <https://zenodo.org/records/1243098>
9. Diem, M., Kleber, F., Fiel, S., Grüning, T., Gatos, B.: cBAD: ICDAR2017 competition on baseline detection. In: *2017 14th IAPR International Conference on Document Analysis and Recognition*. pp. 1355–1360. IEEE (2017). <https://doi.org/10.1109/ICDAR.2017.222>
10. Diem, M., Kleber, F., Sablatnig, R., Gatos, B.: cBAD: ICDAR2019 competition on baseline detection. In: *2019 International Conference on Document Analysis and Recognition*. pp. 1494–1498. IEEE (2019). <https://doi.org/10.1109/ICDAR.2019.00240>
11. Grüning, T., Labahn, R., Diem, M., Kleber, F., Fiel, S.: READ-BAD: A new dataset and evaluation scheme for baseline detection in archival documents. In: *2018 13th IAPR International Workshop on Document Analysis Systems*. pp. 351–356. IEEE (2018). <https://doi.org/10.1109/DAS.2018.38>
12. Grüning, T., Leifert, G., Strauß, T., Michael, J., Labahn, R.: A two-stage method for text line detection in historical documents. *International Journal on Document Analysis and Recognition* **22**(3), 285–302 (2019). <https://doi.org/10.1007/s10032-019-00332-1>
13. Kiessling, B.: A modular region and text line layout analysis system. In: *2020 17th International Conference on Frontiers in Handwriting Recognition*. pp. 313–318. IEEE (2020). <https://doi.org/10.1109/ICFHR2020.2020.00064>
14. Kiessling, B.: CurT: End-to-end text line detection in historical documents with transformers. In: *Frontiers in Handwriting Recognition. Lecture Notes in Computer Science*, vol. 13639, pp. 34–48. Springer (2022). https://doi.org/10.1007/978-3-031-21648-0_3
15. Kodym, O., Hradiš, M.: Page layout analysis system for unconstrained historic documents. In: *Document Analysis and Recognition – ICDAR 2021. Lecture Notes in Computer Science*, vol. 12822, pp. 492–506. Springer (2021). https://doi.org/10.1007/978-3-030-86331-9_32
16. Li, L., Gao, F., Bu, J., Wang, Y., Yu, Z., Zheng, Q.: An end-to-end OCR text re-organization sequence learning for rich-text detail image comprehension. In: *Computer Vision – ECCV 2020*. pp. 85–100. Springer (2020). https://doi.org/10.1007/978-3-030-58595-2_6
17. Likforman-Sulem, L., Zahour, A., Taconet, B.: Text line segmentation of historical documents: A survey. *International Journal on Document Analysis and Recognition* **9**, 123–138 (2007). <https://doi.org/10.1007/s10032-006-0023-z>
18. Lin, T.Y., Goyal, P., Girshick, R., He, K., Dollár, P.: Focal loss for dense object detection. In: *Proceedings of the IEEE International Conference on Computer Vision*. pp. 2980–2988 (2017). <https://doi.org/10.1109/ICCV.2017.324>

19. Liu, S., Li, F., Zhang, H., Yang, X., Qi, X., Su, H., Zhu, J., Zhang, L.: DAB-DETR: Dynamic anchor boxes are better queries for DETR. In: International Conference on Learning Representations (2022)
20. Liu, S., Qi, L., Qin, H., Shi, J., Jia, J.: Path aggregation network for instance segmentation. In: Proceedings of the IEEE Conference on Computer Vision and Pattern Recognition. pp. 8759–8768 (2018). <https://doi.org/10.1109/CVPR.2018.00913>
21. Qiao, L., Li, C., Cheng, Z., Xu, Y., Niu, Y., Li, X.: Reading order detection in visually-rich documents with multi-modal layout-aware relation prediction. *Pattern Recognition* **150**, 110314 (2024). <https://doi.org/10.1016/j.patcog.2024.110314>
22. Quirós, L., Kallio, M., Vidal, E.: Finnish Court Records-sub500. A Dataset of Finnish Notarial Records (19th Century) (2020). <https://doi.org/10.5281/zenodo.3945088>, <https://zenodo.org/records/3945088>
23. Quirós, L., Serrano, L., Bosch, V., Toselli, A.H., Congost, R., Saguer, E., Vidal, E.: Oficio de Hipotecas de Girona. A Dataset of Spanish Notarial Deeds (18th Century) for Handwritten Text Recognition and Layout Analysis of Historical Documents (2018). <https://doi.org/10.5281/zenodo.1322666>, <https://zenodo.org/records/1322666>
24. Quirós, L., Vidal, E.: Reading order detection on handwritten documents. *Neural Computing and Applications* **34**, 9593–9611 (2022). <https://doi.org/10.1007/s00521-022-06948-5>
25. Su, J., Lu, Y., Pan, S., Wen, B., Liu, Y.: Roformer: Enhanced transformer with rotary position embedding. *CoRR* **abs/2104.09864** (2021), <https://arxiv.org/abs/2104.09864>
26. Taghadouini, S., Cavallès, A., Aubertin, B.: LightOnOCR: A 1b end-to-end multilingual vision-language model for state-of-the-art OCR. *arXiv preprint arXiv:2601.14251* (2026). <https://doi.org/10.48550/arXiv.2601.14251>
27. Touvron, H., Lavril, T., Izacard, G., Martinet, X., Lachaux, M.A., Lacroix, T., Rozière, B., Goyal, N., Hambro, E., Azhar, F., Rodriguez, A., Joulin, A., Grave, E., Lample, G.: LLaMA: Open and efficient foundation language models. *arXiv preprint arXiv:2302.13971* (2023). <https://doi.org/10.48550/arXiv.2302.13971>
28. Unter, S.M.: Text line segmentation on ancient egyptian papyri: Layout analysis with object detection networks and connected components. In: Document Analysis and Recognition – ICDAR 2024. *Lecture Notes in Computer Science*, vol. 14806, pp. 215–232. Springer (2024). https://doi.org/10.1007/978-3-031-70543-4_13
29. Vesalainen, A., Mäkelä, E., Ruotsalainen, L., Tolonen, M.: Error patterns in historical OCR: A comparative analysis of TrOCR and a vision–language model. *arXiv preprint arXiv:2602.14524* (2026). <https://doi.org/10.48550/arXiv.2602.14524>
30. Wang, Z., Xu, Y., Cui, L., Shang, J., Wei, F.: LayoutReader: Pre-training of text and layout for reading order detection. In: Proceedings of the 2021 Conference on Empirical Methods in Natural Language Processing. pp. 4735–4744 (2021). <https://doi.org/10.18653/v1/2021.emnlp-main.389>
31. Wignington, C., Tensmeyer, C., Davis, B., Barrett, W., Price, B., Cohen, S.: Start, Follow, Read: End-to-End Full-Page Handwriting Recognition. In: *Computer Vision – ECCV 2018*. pp. 372–388. Springer (2018)
32. Woo, S., Debnath, S., Hu, R., Chen, X., Liu, Z., Kweon, I.S., Xie, S.: ConvNeXt V2: Co-designing and scaling ConvNets with masked autoencoders. In: Proceedings of the IEEE/CVF Conference on Computer Vision and Pattern Recognition. pp. 16133–16142 (2023)

33. Zhao, Y., Lv, W., Xu, S., Wei, J., Wang, G., Dang, Q., Liu, Y., Chen, J.: DETRs Beat YOLOs on Real-time Object Detection. In: Proceedings of the IEEE/CVF Conference on Computer Vision and Pattern Recognition (CVPR). pp. 16965–16974 (June 2024)